Partitioning spatial dynamics in abundance of marine fisheries stocks between fine- and broad-scale variation: a Bayesian approach

E Duskey[a,b,*], DR Hart[c], J-H Chang[c], and PJ Sullivan[d]

[a]Swedish University of Agricultural Sciences, Department of Aquatic Resources, P.O. Box 7050, SE-75007 Uppsala, Sweden
[b]State University of New York College of Environmental Science and Forestry, Department of Environmental and Forest Biology, 1 Forestry Dr, Syracuse, NY 13210, USA
[c]Northeast Fisheries Science Center, 166 Water St, Woods Hole, MA 02543, USA
[d]Cornell University, Department of Natural Resources, 226 Mann Dr, Ithaca, NY 14853, USA
[*]Corresponding author. E-mail: elizabeth.duskey@slu.se

Abstract

Fisheries stocks are often characterized by pronounced spatial patterning. This occurs at different scales, which may be driven by separate mechanisms. Regression kriging is often used to generate population estimates which may parse variation among these scales. A previous application of this and other frequentist methods to estimate the abundance of Atlantic sea scallops (*Placopecten magellanicus*) found that semi-parametric regression kriging performs best among model-based methods. We expanded upon these results by adapting the model structure for a Bayesian framework. This approach demonstrated the trade-off between abundance as a function of depth and broad spatial habitat features, and of fine-scale spatial aggregation. We applied our model to the 2015 belt transect survey of Atlantic sea scallops in Georges Bank and the Mid-Atlantic Bight off the eastern coast of the United States. The overall Bayesian predictions generally agreed with those of the frequentist method. However, the former favored broad spatial trends coupled with very fine-scale aggregation, while the latter favored finer trends and broad aggregation as the dominant driver of scallop abundance. Therefore, one can draw similar conclusions about abundance, yet disparate conclusions about the drivers. Careful consideration of the benefits and limitations of each approach is warranted.

Keywords: Bayesian statistics, regression kriging, generalized additive model, Atlantic sea scallops

1 Introduction

Spatial complexity in nature plays a central role in ecological patterns as fundamental as diversity, and as traditionally applied as spatiotemporal dynamics (Tilman and Kareiva 1997). Patterns may develop at many different scales depending upon the organisms under investigation (Graf et al. 2005). In the marine environment, spatial scale influences genetic diversity (Conover et al. 2006), the nature of density dependence (Shepherd and Litvak 2004), dispersal (Puebla et al. 2012), metacommunity stability (Shackell et al. 2012), and connectivity (Sale and Ludsin 2003). Spatial structure can also have a profound effect on how fisheries stocks respond to fishing, and therefore it is imperative that we include such structure in our assessments (Cadrin and Secor 2009). Explicitly modeling spatial heterogeneity in stock assessment procedures can resolve discrepancies among different areas (Jiao et al. 2016; Truesdell et al. 2016). When unaccounted for, spatial autocorrelation in abundance indices can lead to misrepresentation of precision in estimates (Xu et al. 2018). Potential methods to address this spatial complexity range from relatively simple spatial indexing (Hilborn and Walters 1987) to complex and flexible spatiotemporal models (Cao et al. 2020).

Understanding how and why spatial patterns develop is a critical component of effective fisheries management. In the past, fisheries stocks were treated as homogeneous throughout their range. However, developing technology and local management directives recognize the importance of fine-scale distributions (Wilen 2004). In general, factors influencing populations, including resource availability, competition, and mortality, are all influenced by scale (Levin 1992). A more complete view of fisheries stocks thus requires consideration of interactions with the environment at both fine and broad spatial scales (Ciannelli et al. 2008; Gordon et al. 2018). At fine scales, patchy spatial structure of both community density and removals can have a profound and complex impact on fisheries resources (Barnett et al. 2019). At broader scales, interactions between climate and resource productivity influences catches (Chassot et al. 2010). Management at a range of scales requires both appropriate data and model choice.

Here, we investigate a regression kriging model as a method by which to understand patterns at different spatial scales. With regression kriging, one kriges the residuals of a generalized regression model (Hengl et al. 2007). It represents a potential improvement over many other methods of spatial interpolation (Meng et al. 2013). We developed a Bayesian regression kriging model and compared it to a frequentist model applied to fishery independent survey data on Atlantic sea scallops (*Placopecten magellanicus*). Atlantic sea scallops, hereafter scallops, compose one of the United States' most valuable fisheries, with ex-vessel revenue exceeding $600 million USD in 2021 (NOAA Fisheries 2022). While scallops declined in the mid to late 20th century, area closures, effort reductions and gear restrictions have led to the recovery of the fishery (Hart and Rago 2006). The distribution of scallops is characterized by a very high degree of patchiness (Thouzeau et al. 1991). In order to properly characterize abundance of this and other populations with similar complex spatial distributions, and their driving mechanisms, one must take care to account for all of these processes.

Chang et al. (2017) tested several models on the scallop abundance data, including ordinary kriging (OK), and two variations on semi-parametric regression kriging (RK). They found that regression kriging with a Generalized Additive Model (GAM), termed GAM+OK, performed best among all model-based approaches in terms of both accuracy and precision. The GAM+OK method applies a two stage hurdle GAM to scallop density as a function of depth and two-dimensional spatial coordinates. The residuals of this model are then used to perform ordinary kriging. Conceptually, this model describes a broad trend with depth, and in space, and describes what remains as a function of spatial aggregation. While more complex and computationally demanding than either method alone, one of the advantages of this and similar approaches is that one takes advantage of all available information (Hengl et al. 2007). Scallops tend to occupy intermediate depths. At shallow depths, maximum bottom temperatures may exceed the temperatures at which the scallops can survive (Hart and Chute 2004). In deeper waters, scallop recruitment is inhibited both by limited food resources and, in some areas, predation by

Astropecten sea stars (Hart 2006; Shank et al. 2012). In space, broad trends may follow sediment type or tidal and other current transport mechanisms (Thouzeau et al. 1991). At smaller spatial scales, scallops may enhance their own recruitment directly by aggregating as fecund adults (Caddy 1970; Stokesbury and Himmelman 1993). Therefore, each piece of this model is designed to describe a different, though not entirely separate, mechanism. A challenge exists, however, in that the scales of the regression and geostatistical models may overlap, and thus the results may be highly autocorrelated. For example, water depth is itself related to the spatial coordinates. How, then, do we determine the proportion of observed variation attributable to each process?

With the GAM+OK method, the model first finds an optimal fit to observations as a function of depth and two-dimensional space. As a natural result of the fitting methods, the model will attempt to find an unbiased fit of the smoothing functions to the data. One then fits a variogram to the residuals that remain. Because of the subsequent application of models, overfitting and therefore bias in the estimates can result due to the lack of an iterative reweighting or other recursive scheme. By contrast, in a Bayesian framework, we can find an optimal fit to all pieces simultaneously by sampling from a joint likelihood (Raftery et al. 1992), which may reduce the potential for overfitting by the GAM. Bayesian models have several advantages, including a natural structure for prior information and probabilistic interpretability (Grzenda 2015; Wagenmakers et al. 2016). There are many years of survey data on the scallop, and a great deal of biological data concerning the animals' physiology and behavior (Hart and Chute 2004). This includes extensive knowledge of growth and reproductive rates (Naidu and Robert 2006; Hart and Chute 2009), as well as spatial trends (Thouzeau et al. 1991; Hart 2006; Chang et al. 2017). However, these models can produce an infinite estimation space (Ginsbourger et al. 2009) and thus induce collinearity. One can mitigate this by appropriate choice of prior distributions, and by application of model restrictions that reflect our knowledge of the system (Lemoine 2019). Other methods, including maximum marginal likelihood (Miller 2013; Miller et al. 2019) and delta-generalized linear mixed models (Thorson et al. 2015), may also parse probability of presence, conditional

mean abundance, and spatial variation, but we focus on a Bayesian approach here.

In this paper, we analyzed spatial scallop abundance data provided in Chang et al. (2017) using a Bayesian geostatistical framework, and examine both its potential faults and theoretical gains in comparison to a frequentist counterpart. Ultimately, we would like to use this model to produce informative estimates for subsequent years, augmented by one year of growth and reproduction. Informative priors can be robust to inaccurate information (Depaoli 2014), avoid problems associated with non-informative priors when data are relatively sparse (Lenk and Orme 2009), and can easily be adjusted to reflect the degree of confidence in one's past information (Horrocks and Rueffer 2014). This could serve as a powerful framework for analysis of spatiotemporal survey data.

2 Methods

2.1 Data Overview

The Woods Hole Oceanographic Institution (WHOI), the Northeast Fisheries Science Center (NEFSC), and commercial fishermen developed the Habitat Camera Mapping System (HabCam) to survey benthic communities in general, and scallops in particular (Howland et al. 2006; Chang et al. 2017; Kaplan et al. 2017; Kaplan et al. 2018). Region-scale HabCam surveys were conducted on Georges Bank (GB) in 2011, and in both GB and the Mid-Atlantic Bight (MAB) in the summer of 2012-2019 and 2021-2022 (Figure 1). The HabCam vehicle took roughly six photographs per second as it was towed along pre-designed transects at a height of about 2m off the sea floor. Sampling design included both long and short transects, with long transects in the direction of the density gradient that reach to sampling area boundaries coupled with short transects over high density areas (NEFSC 2014). This design concentrated sampling in higher density areas and allowed for the estimation of anisotropy. Researchers manually annotated a subset of about 100,000 images per year (roughly 2% of the total), counting both juveniles and adults. We

aggregated these data at the scale of 5km segments to reduce the number of observations and the degree of autocorrelation, thereby reducing the computational burden on the models. The surveys in each region were stratified into subareas (seven in GB and five in MAB) in order to obtain areas with more homogeneous relationships of scallops with depth. As in Chang et al. (2017), we ran our model separately in each area.

Our species of interest, the Atlantic sea scallop, can be found off the Atlantic coast of the United States from Cape Hatteras in North Carolina up to Newfoundland (Hart and Rago 2006). They are a relatively long-lived (maximum age about 20 years), fast-growing bivalve mollusc of great commercial importance, particularly in recent years (NEFSC 2018). Their population dynamics can be characterized by an affinity for sand and gravel bottoms, intermediate depths, and avoidance of sea star predators (Thouzeau et al. 1991; Hart and Chute 2004). They become sexually mature at age two, but do not recruit to the fishery or contribute substantially to spawning until age four (NEFSC 2014). Synchronous spawning typically occurs from August-October, although spawning may also occur in April-June in certain areas (Hart and Chute 2004). Adults range in size from 80-170 mm. Food availability and temperature are primary determinants of individual growth potential (Cranford et al. 1998). Ideal temperatures for Atlantic sea scallops range from 8-15°C, with mortality occurring over 21°C (Hart and Chute 2004). Within the Mid-Atlantic Bight and Georges Bank, temperature preference is a major driver of depth range of individuals, though this may be constrained by interactions with predators (Hart 2006). In the Mid-Atlantic Bight, major south-going currents transport scallop larvae, and fishery closures have induced strong recruitment in down-current areas (Hart et al. 2020). Similar dynamics occur in the circular currents in Georges Bank (Chen et al. 2021).

We chose to analyze data from the year 2015. Data from this year exhibited exceptional coverage and contrast. It thus serves as a good case study. Examining annual variation is outside the scope of the current study. We do however recommend examining temporal effects as the logical next step of this research.

2.2 Estimation Model

We built a Bayesian extension of the GAM+OK method described in Chang et al. (2017) in **Stan** (Carpenter et al. 2017). This regression kriging method consists of a GAM for the mean and ordinary kriging on the resulting residuals, described below.

2.2.1 Generalized additive model

Generalized additive models (GAM's) are used to identify nonlinear covariate effects (Hastie and Tibshirani 1990). We used a zero-inflated negative binomial generalized additive model to describe mean scallop abundance, which can be written:

$$y_i \sim \begin{cases} (1-\boldsymbol{\pi}) + \boldsymbol{\pi} \cdot \mathsf{NB}(0,\phi) & \text{if } y_i = 0 \\ \boldsymbol{\pi} \cdot \mathsf{NB}(\mu,\phi) & \text{if } y_i > 0 \end{cases} \tag{1}$$

The observations are given by $y_i \in \boldsymbol{y}$, and $\pi_i \in \boldsymbol{\pi}$ is the probability of presence at location i. Following Chang et al. (2017), we used cubic splines to smooth over depth. We used a low rank, truncated basis for the cubic spline as a function of depth (Crainiceanu et al. 2005), with K_d knots spaced evenly throughout the range of the data. We also included a two-dimensional thin plate spline (Wood 2003) on abundance as a function of spatial coordinates. Here, we used hierarchical clustering to place observations into K_c groups based on distance using the `hclust` and `cutree` functions in R (R Core Team 2022), and calculated the mean location of each group to assign the K_c knot locations. Our approach to knot placement differs from the default used by the R package **mgcv**, which uses generalized cross-validation (Wood 2003). However, knot number and location are generally not critical as long as there is adequate data coverage and knot numbers exceed degrees of freedom plus one (Wood 2001). We set $K_d = 5$ and $K_c = 15$ as in Chang et al. (2017) for all models, which ensured this was the case. The use of hierarchical clustering is non-standard, but it does ensure good spatial coverage. Therefore, we do not expect large difference between our approach and that of Chang et al. (2017) due to these differences.

The expectation of each observation can be written:

$$E[\boldsymbol{y}] = \exp\left(\boldsymbol{B}\boldsymbol{b} + \text{offset}\right) \tag{2}$$

with a design matrix $\boldsymbol{B}$ and coefficients $\boldsymbol{b} = \{\boldsymbol{b}_{K_d}, \boldsymbol{b}_{K_c}\}$, where $\boldsymbol{b}_{K_d}$ gives the coefficients of the cubic spline with depth and $\boldsymbol{b}_{K_c}$ gives the coefficients of the thin plate spline with two-dimensional space. The offset gives the area of each observation in square meters. We set the following priors for $\boldsymbol{b}_{K_d}$ and $\boldsymbol{b}_{K_c}$, and their associated variances:

$$\begin{aligned} \boldsymbol{b}_{K_d} &\sim N(0, \sigma_d^2) \\ \boldsymbol{b}_{K_c} &\sim N(0, \sigma_c^2) \\ \sigma_d^2,\, \sigma_c^2 &\sim N(0,1)\, T[0,] \end{aligned} \tag{3}$$

where the distribution $N(0,1)\,T[0,]$ indicates a standard normal distribution truncated below at 0, and where σ_d^2 and σ_c^2 are products of the variance and the inverse of the penalty of each spline function (Crainiceanu et al. 2005).

We gave the overdispersion parameter ϕ of equation 1 the prior:

$$\phi \sim \text{Gamma}(1, 0.5) \tag{4}$$

Presence for the i^{th} observation is a function of spatial coordinates. Scallop presence tends to correlate with depth (Thouzeau et al. 1991; Hart 2006), which itself is highly correlated with spatial coordinates. Thus, we modeled presence as a simple Gaussian function of the coordinate direction with the greatest range of observed depths:

$$\pi_i = a\, \exp\left(-(x_i - k)^2/s\right) \tag{5}$$

where x_i represents either scaled longitude or latitude. Choosing just one of these as covariates avoids additional computational burdens and collinearity resulting in poor model diagnostics. Similarly, depth alone resulted in a reduction in predictive power and poor diagnostics. Note that our model structure assumes that probability of presence is constant in the discarded coordinate value. While this may be restrictive, additional variability over both spatial coordinates and depth are captured in the mean process. We gave the coefficients in equation 5 the following priors:

$$\begin{aligned} a &\sim \text{Uniform}(0, 1) \\ k &\sim N(0, 1) \\ s &\sim \text{Gamma}(1, 5) \end{aligned} \tag{6}$$

Note that this differs from the model in Chang et al. (2017), in which presence was included in a hurdle model. In practice, we have found that hurdle models can be difficult to fit with Stan. Using the zero-inflated model improved both computation time and diagnostics. Note that the zeroes in the zero-inflated model are treated as either structural or sampling. Structural zeroes arise from a binomial model component, whereas sampling zeroes may arise by chance from the count model component (Feng 2021). By contrast, hurdle models consider zeroes and non-zeroes separately in a mixture-type structure. For the former, non-presence in unsuitable areas is modeled as structural and non-presence in suitable areas is modeled as a chance event. For hurdle models, non-presence arises from just one structural source. Here, all zeroes are considered to arise from unsuitability. Comparisons of both models indicate the zero-inflated model may be more appropriate for the scallop data, given high contrast in zeroes across the sampling area (Feng 2021).

Ultimately, the procedure described above produced mean estimates $\mu_i \in \boldsymbol{\mu}$, which were used to calculate the model residuals.

2.2.2 Kriging

Given the residuals $\boldsymbol{\epsilon}$ arising from the GAM, we wished to predict the residual at a new point, given by ϵ_0, as a weighted sum of the observed residuals ϵ_i as follows:

$$\hat{\epsilon}_0 = Z(\epsilon_0) = \sum_{i=1}^{N} w_i \epsilon_i = \boldsymbol{w}^T \boldsymbol{\epsilon} \tag{7}$$

The weights w_i of the variogram are a function of the variance-covariance matrix of the residuals from the GAM and of the covariance of the observations ϵ_i with the unobserved quantity ϵ_0. The structure of this matrix is typically given by one of several variograms, a conditionally negative definite function which asserts that data points that are closer together are more closely related. Chang et al. (2017) used a Matérn variogram. However for ease of computation within **Stan**, we used the exponential variogram, a special case of the Matérn:

$$\text{Cov}(\epsilon_i, \epsilon_j) = \text{nugget} + \text{sill} \, \exp\left(-||\epsilon_i - \epsilon_j||/\text{range}\right) \tag{8}$$

where $h = ||\cdot||$ is the Euclidean distance. We chose the following priors for the variogram parameters:

$$\begin{aligned} \text{nugget} &\sim N(0,1)\, T[0,] \\ \text{sill} &\sim N(0,1000)\, T[0,] \\ \text{range} &\sim N(0,1)\, T[0,] \\ \mu_{\epsilon_i} &\sim N(0,1) \end{aligned} \tag{9}$$

where, as in equation 3 above, $T[0,]$ indicates truncation below at zero. The nugget represents semi-variance at zero distance, or rather the local variance. Local variance is also given by the parameters σ_d^2 and σ_c^2. This parameter is often not estimated i.e. remains nearly identical to the prior. We chose a relatively small and constrained prior for the nugget. The sill represents maximum semi-variance at distances past the range. This can take on a wide range of positive values, and therefore we chose an uninformative truncated normal prior. The range represents

the distance at which semi-variance begins to saturate. The distances have been scaled and do not exceed a value of three. Thus, the constrained truncated normal is relatively uninformative in the context of the support.

The likelihood for this model is given by:

$$\boldsymbol{\epsilon} \sim \text{MVN}(\mu_{\boldsymbol{\epsilon}}, \boldsymbol{C}) \tag{10}$$

where MVN is the multivariate normal distribution with variance-covariance matrix given by equation 8. The estimated totals are:

$$\hat{\boldsymbol{y}} = \hat{\boldsymbol{\mu}} + \hat{\boldsymbol{\epsilon}} \tag{11}$$

where each $\hat{\mu_i} \in \boldsymbol{\mu}$ arises from the GAM given that it is non-zero, and each $\hat{\epsilon_i} \in \boldsymbol{\epsilon}$ arises from the variogram.

2.3 Implementation

We ran the Bayesian model, which we refer to as Bayes+OK, in **Stan** (Carpenter et al. 2017) using the package **cmdstanr** (Gabry and Češnovar 2021) in R (R Core Team 2022). In each of the 12 depth-stratified areas (NEFSC 2014), the model was run for 2,000 iterations over 6 chains, with the first 1,000 discarded for warmup, for a total of 6,000 samples. The models ran for an average of 113 minutes, with completion times ranging from 13 to 250 minutes. Each model converged, with Gelman-Rubin diagnostics of all parameters $\hat{R} < 1.1$. All parameters of each model had sufficient effective sampling sizes of more than 100 for the both the bulk and the tail, indicating adequate sampling of the mean and median, and of the upper and lower quantiles. Visual inspection of each chain of all parameters were indicative of good mixing. All models were run with 5 knots for the depth smoother and 15 knots for the spatial coordinate smoother, to coincide with knot choices made by Chang et al. (2017). For the purpose of comparison, we also re-ran the GAM+OK model described in Chang et al. (2017) on the data aggregated at a 5km

scale.

To compare the performance of both models, we implemented a standard 10-fold cross-validation procedure (Rodriguez et al. 2009) and calculated the root mean square error (RMSE) of each subarea $j \in \{1, , , J\}$ as follows:

$$\text{RMSE} = \sqrt{\frac{\sum_{j=1}^{J} \sum_{i=1}^{N_j} (\hat{x_i} - x_i)^2}{N}} \tag{12}$$

For the GAM+OK, we used ordinary least squares to estimate the parameters of a Matérn variogram with no anisotropy. We also ran a sensitivity analysis on prior choice of certain model parameters, which we present in the Supplementary Materials section.

3 Results

Overall, the Bayes+OK model proved stable and efficient. The abundance results of our model agreed fairly well with the results of the GAM+OK or the stratified mean (SM) given by assessment results (NEFSC 2018, Table 1). Below, we present the results of each piece of the model individually for clarity, followed by summary totals in each area of Georges Bank (GB) and the Mid-Altantic Bight (MAB).

3.1 Probability of presence

Recall that we modeled presence as a Gaussian function of a cardinal direction (equation 5). In most cases, it was clear that there was a strong relationship between cardinal direction and probability of presence (Figure 2). There were exceptions, in that the minimum and maximum mean probability were similar, particularly in Delmarva (DMV), reflecting a relatively consistently high probability of presence throughout this area. Even so, generally each area tended to have a varied and complex relationship of presence with location, often represented by a strong preference

for a central region, or an extreme.

Our intention was to allow the cardinal coordinate to serve in part as a proxy for depth, while also allowing for some spatial variability. Visually, we could associate the estimated probability of presence with observed depth (Figure 2; see also Figure S1). In some areas, as in Hudson Canyon (HC), presence peaked at central longitudes, where depth is roughly between 40m and 80m. In other areas, the preference appeared to be for relatively deep waters. For example, in Closed Area 2 North (CA2_N), probability of presence increased toward the north, where depths exceed 65m. In the case of Delmarva (DMV), there were clear and substantial differences in depth throughout the area, yet little apparent preference for a given spatial extent, with only small evidence of avoidance of the western and eastern extremes.

3.2 Mean Abundance

To understand the contributions of depth and spatial coordinates to mean abundance, the design matrix $\boldsymbol{B}$ was split into its depth and coordinate components, written here as $\boldsymbol{B}_d$ and $\boldsymbol{B}_c$, respectively. Thus, estimated mean abundance can be expressed as:

$$\hat{\boldsymbol{y}} = \hat{\boldsymbol{y}}_d \cdot \hat{\boldsymbol{y}}_c \tag{13}$$

where

$$\hat{\boldsymbol{y}}_d = \exp\left(\boldsymbol{b}_{K_d}\boldsymbol{B}_d\right) \tag{14}$$

$$\hat{\boldsymbol{y}}_c = \exp\left(\boldsymbol{b}_{K_c}\boldsymbol{B}_c\right) \tag{15}$$

and $\boldsymbol{b}_{K_d}$ and $\boldsymbol{b}_{K_c}$ are the components of $\boldsymbol{b}$ in equation 3.

In general abundance peaked at intermediate depths, with abundance approaching zero at the extremes (Figure 3). Note that mean estimates may not match observed trends. When this occurs, discrepancies are explained by spatial covariance, or large masses of individuals clustering

in beds. Peaks in mean abundance at intermediate depths was fairly universal throughout each area of each region, though in some areas, depth preference was near the observed extremes, as in Southern Flank (SF), or increased slightly towards the extremes, as in Hudson Canyon southern rim (HCsr). When we considered the impact of two-dimensional spatial coordinates alone on abundance, we found that mean estimates varied considerably, often with sharp peaks in high abundance locations (Figure 4). In a few areas, changes in abundance with space were more gradual. The tendency towards patchiness in some areas was likely due to the use of a relatively higher number of knots. The cardinal coordinates were, of course, an indirect measure of other variables that varied over space. This could include habitat at a broader scale, which was our intention, or other variables, such as presence of competitors or predators. The results of the GAM+OK are visibly patchier in both the Mid-Atlantic Bight and Georges Bank (Figures 5 and 6; see also Figure S2). That is, the frequentist model assigns more fine-scale variability to the mean process than the Bayesian model.

3.3 Residuals

Estimated variogram parameters were very different between the frequentist and Bayesian methods (Table 1). Estimated sills arising from the Bayesian method were generally much higher than those arising from the frequentist method. The opposite was true for the range. Thus, our Bayes+OK model suggested that autocorrelation was a very strong force driving very localized abundance, whereas the GAM+OK model suggested that aggregation occurred at much broader scales, and was relatively weak. While both models give patchy results, the Bayes+OK kriged residuals are comparatively smoother than the GAM+OK kriged residuals in some areas (Figures 5 and 6; see also Figure S3). The reverse is true in other areas, indicating that the character of the estimated residuals is dependent upon the region. Given that the mean process differed in each region and between models, these results were not surprising.

Note that the nuggets of the Bayes+OK model were all very similar, and were in fact roughly equal to the mean of its prior. We found that nugget posteriors were equal to the priors no matter our choice of variance, indicating the model did not truly estimate the nugget. This may be due to the inclusion of variance-inverse penalty hyperparameters, which also described variability with both depth and space. Also of note is that the coefficient of variation (CV) of the abundance estimates were typically lower for the Bayesian model. Thus, the Bayes+OK model was more precise, though not necessarily more accurate.

3.4 Cross-validation

The 10-fold cross-validation procedure indicated that, on average, the Bayes+OK model (RMSE $= 3.95$) performed slightly better than the GAM+OK (RMSE $= 3.99$). Results also indicated that the Bayes+OK model performed best in 67% of the subareas, and was bested by the GAM+OK most often in Georges Bank. That said, cross-validation generally supports the Bayes+OK over GAM+OK.

4 Discussion

Determining the mechanisms driving spatial patterns of abundance of marine species at various scales is a difficult undertaking. Regression kriging is capable of providing estimates of the contribution of different processes to spatial variation. However, the conclusions to be drawn clearly differ by method of application. In general, our Bayesian model interpreted scallop abundance as a smooth mean process with a very high magnitude of spatial autocorrelation at very fine scales. While the mean process alone would suggest high abundance at intermediate depths, the tendency to cluster at finer scales may produce peaks in relatively less suitable regions. By contrast, the GAM+OK method suggested broader autocorrelation and highly nonlinear trends. Which of these models is "better" may be a matter of context. Cross-validation generally supports the Bayes+OK model, though by a relatively fine margin, and only among a majority of subareas

(Figure 7). The GAM+OK model may naturally attribute more of the variation to trend because the GAM is applied first. The Bayesian approach is advantageous in that it estimates the GAM and kriging parts simultaneously, thus balancing these two components. Unbiased priors would increase the precision and accuracy of the estimates, but poor choices of priors could induce bias. One may influence the GAM by judicious choice of a variance-inverse penalty prior, the number of knots, and the priors for the parameters of the variogram. This flexibility may not be best for situations in which little is known about the mechanisms driving the distribution of a given species, though median estimates do appear to be fairly robust to the choice of priors (see Figure S5). Fortunately, we do have prior information on the mechanisms guiding the abundance of scallops. Therefore, in our case, and in similar cases, the Bayes+OK model may be an appropriate method by which to estimate abundance and its constituents.

Note that, while the models are not directly comparable, given we use somewhat different methods to accomodate both the strengths and limitation of Stan and **mgcv**, we chose to compare models based on k-fold cross-validation. This and other methods of cross-validation transcend differences among models to emphasize the ability of different models to make predictions. While it is still difficult to say which model is more correct overall, we can corroborate some results. For example, the GAM+OK model suggests there may be high abundance within the deepest portions of the Hudson shelf valley, whereas the Bayes+OK model suggests there are very few scallops present in this area (Figure 5; see also Figure S4). We know from observational data that the latter is more correct, as these deep waters are unsuitable for the scallops due to high abundance of *Astropecten* sea star predators (Hart 2006; Shank et al. 2012). The results of the cross-validation procedure provide evidence in favor of our accepting the conclusions of the Bayes+OK model in this region over those of the GAM+OK (Figure 7). It may not be appropriate to do so in situations in which there is very little knowledge of the species in question. We felt this model was appropriate for scallops, especially considering that, despite variability in explanatory processes with prior choice, mean and residual density estimates remained the same (see Figure

S5). Furthermore, a sensitivity analysis on the choice of priors suggests that the results of the Bayes+OK model are robust (Supplement S2; see Figure S5). Thus, several methods of validation may aid one in choosing between the models presented here.

While the availability of priors is an advantage of Bayesian methods, there is a delicate balance between choosing model priors that give good diagnostics in a reasonable amount of time and choosing model priors based on known quantities. Our current parameterization may err on the side of sacrificing some realism for swift convergence. For example, we chose a low variance for mean residuals because a less restrictive prior resulted in slow exploration of a highly auto-correlated space. This also invariably led to flatter penalized splines and greater autocorrelation at broader scales. That is, given that this model is designed to attribute a proportion of the observations to trend, and that which remains to spatial aggregation, decreasing the flexibility of the former increases the flexibility of the latter. Allowing greater flexibility in the variance-inverse penalty did the reverse – the GAM had more explanatory power while the variogram parameters shrunk. Allowing flexibility in both resulted in very long run times and poor diagnostics. One can potentially arrive at an infinite number of solutions based on these or other restrictions within the model and therefore, interpretations must be treated with caution, and tempered by expert knowledge.

We believe the Bayes+OK represents an improvement over the GAM+OK. Though **Stan** is an exceptionally fast and flexible tool for repeated sampling in a Bayesian context, it can still be burdened by high computational costs. In future studies, integrative nested Laplace approximation (INLA) may be an attractive alternative (Bakka et al. 2018). Though applications are somewhat limited by model assumptions, INLA allows for simultaneous Bayesian estimation of spatial and temporal relationships, whether parametric or semi- or non-parametric. Future studies may wish to compare our methods with those used for this and other marine species (Izquierdo et al. 2021; Outeiro et al. 2021). This may represent an additional improvement over the Bayes+OK model. While it does perform relatively well, there are still some results arising from the former that

contradict expectations. The spatial scales suggested by the Bayesian estimates of the ranges of the variogram were likely small compared to the GAM+OK estimates because of the direct interaction of the GAM with the variogram, as expected. That said, we also expected somewhat greater ranges in the case of some of the areas with large aggregations (Table 1). In future runs, we or others may wish to inform the priors of likely range values until we arrive at estimates more consistent with observations and expert knowledge. While it may be difficult to interpret individual GAM coefficients, the overall pattern they produce over depth and in space can be informed by observations, and can become either more or less flexible by tweaking the associated variance-inverse penalties. The sill and especially the range of the variogram have a more direct biological interpretation. We can use prior information concerning aggregative behavior as a check on kriging model output. Scallops form aggregations over the bottom substrate, and to different degrees depending on region and age (Caddy 1970; Carey and Stokesbury 2011). Information of this sort can be used to reconcile model predictions with observations.

Similarly, prior information on the species in question can be used to interpret model results. For Atlantic sea scallops, broad trends with very fine-scale autocorrelation aligns with knowledge of behavior and life history. For example, fine-scale behavior and aggregations influence fertilization success and dispersal (Bayer et al. 2018; Chen et al. 2021). At much broader scales, substrate type and oceanographic conditions influence larval survival, success, and transport (Thouzeau et al. 1991; Chen et al. 2021). These relationships are generally captured by the inclusion of coordinates in the mean and presence-absence processes. HabCam images do include substrate information (for example, sand, sand/gravel, gravel, cobble etc). However, when included in the models, the effects of substrate on abundance is minimal. Images are annotated for the the scallop predator *Cancer* spp., but these predators have limited effects on scallop populations (Hart 2006; Shank et al. 2012). Additionally, there are currently no estimates of predator abundance outside of the sampled transects. Therefore, we would be unable to extrapolate scallop abundance throughout each area. It is possible previously established relationships could change somewhat

with application of our model, and so we recommend that potential methods of extrapolation for environmental conditions and predators be explored in future studies.

One of the primary advantage of the Bayes+OK method is that there is a formal structure by which to include expert knowledge as prior information. Our next goal, to inform estimates of abundance in subsequent years, can also be achieved by taking advantage of prior distributions. We can apply an observed size distribution and average growth and fecundity rates to the following years' estimates, or alternatively can including temporal structure into the flexible framework (e.g. Bauer et al. 2016). Temporal applications can also be explored with INLA (Bakka et al. 2018). Any restrictions introduced into the model serve as a form of prior belief, and so we cannot necessarily say that we have confirmed that each of these processes – depth preference, spatial trend, small-scale aggregation – described by the GAM and by the variogram act on the exact scales predicted by either the Bayes+OK or the GAM+OK method. However, we applied these restrictions because we do have good, prior information about scallop distribution, abundance, and ecology, based in part on previous surveys. This is precisely the situation for which informative priors were designed. Generally speaking, the Bayesian model did behave well when we included restrictive priors on the variance-inverse penalty of the GAM and the local mean of the residuals, which is some evidence that it was an appropriate structure. The general robustness of the results to prior choices corroborates this (Supplement S2). The fact that it also offered similar estimates with very different output for the parameters suggests that, in actuality, more of the process is attributable to fine-scale spatial autocorrelation than originally suggested by the GAM+OK method.

5 Conclusions

Overall, we believe the Bayes+OK method is a strong and viable model structure, particularly when use of prior information is employed. It can be applied to any spatial fisheries data collected at a relatively fine scale, with or without covariate drivers in addition to space itself. Given

that the Bayes+OK model includes a scheme by which both the parameters of the GAM and of the variogram are estimated simultaneously, our results sugges it is a more biologically accurate representation of the processes driving patterns of abundance and density. This approach can not only improve assessments of fisheries stocks, but also allow us to target management actions at multiple spatial scales.

Author contributions

ED, DH, J-HC, and PJ conceived of the study. ED, DH, and J-HC designed the analysis. ED wrote the code, with significant input from PJ. ED wrote the manuscript and DH, J-HC, and PJ contributed to the editing of all drafts. All authors gave final approval for publication.

Declaration of competing interest

The authors declare there are no competing interests.

Data availability statement

The scallop survey dredge data used in this study are available at https://catalog.data.gov/dataset/sea-scallop-survey.

References

Bakka, H., Rue, H., Fuglstad, G.-A., Riebler, A., Bolin, D., Illian, J., Krainski, E., Simpson, D., and Lindgren, F. (2018). "Spatial modeling with R-INLA: A review". In: *WIREs Computational Statistics* 10.6, e1443. DOI: https://doi.org/10.1002/wics.1443.

Barnett, L. A., Ward, E. J., Jannot, J. E., and Shelton, A. O. (2019). "Dynamic spatial heterogeneity reveals interdependence of marine faunal density and fishery removals". In: *Ecological Indicators* 107, p. 105585. ISSN: 1470-160X. DOI: https://doi.org/10.1016/j.ecolind.2019.105585.

Bauer, C., Wakefield, J., Rue, H., Self, S., Feng, Z., and Wang, Y. (2016). "Bayesian penalized spline models for the analysis of spatio-temporal count data". In: *Statistics in Medicine* 35.11, pp. 1848–1865. DOI: 10.1002/sim.6785.

Bayer, S. R., Wahle, R. A., Brady, D. C., Jumars, P. A., Stokesbury, K. D. E., and Carey, J. D. (2018). "Fertilization success in scallop aggregations: reconciling model predictions and field measurements of density effects". In: *Ecosphere* 9.8, e02359. DOI: https://doi.org/10.1002/ecs2.2359.

Caddy, J. (1970). "A method of surveying scallop populations from a submersible". In: *Journal of the Fisheries Board of Canada* 27.3, pp. 535–549. DOI: 10.1139/f70-057.

Cadrin, S. X. and Secor, D. H. (2009). "Accounting for spatial population structure in stock assessment: past, present, and future". In: *The future of fisheries science in North America*. Springer, pp. 405–426. DOI: 10.1007/978-1-4020-9210-7_22.

Cao, J., Thorson, J. T., Punt, A. E., and Szuwalski, C. (2020). "A novel spatiotemporal stock assessment framework to better address fine-scale species distributions: development and simulation testing". In: *Fish and Fisheries* 21.2, pp. 350–367. DOI: 10.1111/faf.12433.

Carey, J. D. and Stokesbury, K. D. (2011). "An assessment of juvenile and adult sea scallop, *Placopecten magellanicus*, distribution in the northwest Atlantic using high-resolution still imagery". In: *Journal of Shellfish Research* 30.3, pp. 569–582. DOI: 10.2983/035.030.0301.

Carpenter, B., Gelman, A., Hoffman, M. D., Lee, D., Goodrich, B., Betancourt, M., Brubaker, M. A., Guo, J., Li, P., and Riddell, A. (2017). "Stan: a probabilistic programming language." In: *Grantee Submission* 76.1, pp. 1–32. DOI: 10.18637/jss.v076.i01.

Chang, J.-H., Shank, B. V., and Hart, D. R. (2017). "A comparison of methods to estimate abundance and biomass from belt transect surveys". In: *Limnology and Oceanography: Methods* 15.5, pp. 480–494. DOI: 10.1002/lom3.10174.

Chassot, E., Bonhommeau, S., Dulvy, N. K., Mélin, F., Watson, R., Gascuel, D., and Le Pape, O. (2010). "Global marine primary production constrains fisheries catches". In: *Ecology Letters* 13.4, pp. 495–505. DOI: https://doi.org/10.1111/j.1461-0248.2010.01443.x.

Chen, C., Zhao, L., Gallager, S., Ji, R., He, P., Davis, C., Beardsley, R. C., Hart, D., Gentleman, W. C., Wang, L., Li, S., Lin, H., Stokesbury, K., and Bethoney, D. (2021). "Impact of larval behaviors on dispersal and connectivity of sea scallop larvae over the northeast U.S. shelf". In: *Progress in Oceanography* 195, p. 102604. ISSN: 0079-6611. DOI: https://doi.org/10.1016/j.pocean.2021.102604.

Ciannelli, L., Fauchald, P., Chan, K., Agostini, V., and Dingsør, G. (2008). "Spatial fisheries ecology: Recent progress and future prospects". In: *Journal of Marine Systems* 71.3. The Wrapping Up of the IDEA Project: pp. 223–236. ISSN: 0924-7963. DOI: https://doi.org/10.1016/j.jmarsys.2007.02.031.

Conover, D., Clarke, L., Munch, S., and Wagner, G. (2006). "Spatial and temporal scales of adaptive divergence in marine fishes and the implications for conservation". In: *Journal of Fish Biology* 69, pp. 21–47. DOI: 10.1111/j.1095-8649.2006.01274.x.

Crainiceanu, C., Ruppert, D., and Wand, M. P. (2005). "Bayesian analysis for penalized spline regression using WinBUGS". In: *Faculty of Engineering and Information Sciences - Papers: Part A* 2517. URL: https://ro.uow.edu.au/eispapers/2517.

Cranford, P., Emerson, C., Hargrave, B., and Milligan, T. (1998). "In situ feeding and absorption responses of sea scallops *Placopecten magellanicus* (Gmelin) to storm-induced

changes in the quantity and composition of the seston". In: *Journal of Experimental Marine Biology and Ecology* 219.1, pp. 45–70. ISSN: 0022-0981. DOI: https://doi.org/10.1016/S0022-0981(97)00174-3.

Depaoli, S. (2014). "The impact of inaccurate "informative" priors for growth parameters in Bayesian growth mixture modeling". In: *Structural Equation Modeling: A Multidisciplinary Journal* 21.2, pp. 239–252. DOI: 10.1080/10705511.2014.882686.

Feng, C. X. (2021). "A comparison of zero-inflated and hurdle models for modeling zero-inflated count data". In: *Journal of Statistical Distributions and Applications* 8.1, p. 8. ISSN: 2195-5832. DOI: 10.1186/s40488-021-00121-4.

Gabry, J. and Cešnovar, R. (2021). *cmdstanr: R Interface to 'CmdStan'*. https://mc-stan.org/cmdstanr, https://discourse.mc-stan.org.

Ginsbourger, D., Dupuy, D., Badea, A., Carraro, L., and Roustant, O. (2009). "A note on the choice and the estimation of kriging models for the analysis of deterministic computer experiments". In: *Applied Stochastic Models in Business and Industry* 25.2, pp. 115–131. DOI: 10.1002/asmb.741.

Gordon, T. A. C., Harding, H. R., Clever, F. K., Davidson, I. K., Davison, W., Montgomery, D. W., Weatherhead, R. C., Windsor, F. M., Armstrong, J. D., Bardonnet, A., Bergman, E., Britton, J. R., Côté, I. M., D'agostino, D., Greenberg, L. A., Harborne, A. R., Kahilainen, K. K., Metcalfe, N. B., Mills, S. C., Milner, N. J., Mittermayer, F. H., Montorio, L., Nedelec, S. L., Prokkola, J. M., Rutterford, L. A., Salvanes, A. G. V., Simpson, S. D., Vainikka, A., Pinnegar, J. K., and Santos, E. M. (2018). "Fishes in a changing world: learning from the past to promote sustainability of fish populations". In: *Journal of Fish Biology* 92.3, pp. 804–827. DOI: https://doi.org/10.1111/jfb.13546.

Graf, R. F., Bollmann, K., Suter, W., and Bugmann, H. (2005). "The importance of spatial scale in habitat models: capercaillie in the Swiss Alps". In: *Landscape Ecology* 20.6, pp. 703–717. DOI: 10.1007/s10980-005-0063-7.

Grzenda, W. (2015). "The advantages of Bayesian methods over classical methods in the context of credible intervals". In: *Information Systems in Management* 4. bwmeta1.element.baztech-df752911-e9a2-40c6-a725-27d2d5f024ca.

Hart, D. and Chute, A. (2004). "Essential fish habitat source document: sea scallop". In: *Placopecten magellanicus, life history and habitat characteristics*.

Hart, D. R. (2006). "Effects of sea stars and crabs on sea scallop *Placopecten magellanicus* recruitment in theMid-Atlantic Bight (USA)". In: *Marine Ecology Progress Series* 306, pp. 209–221. DOI: 10.3354/meps306209.

Hart, D. R. and Chute, A. S. (2009). "Estimating von Bertalanffy growth parameters from growth increment data using a linear mixed-effects model, with an application to the sea scallop *Placopecten magellanicus*". In: *ICES Journal of Marine Science* 66.10, pp. 2165–2175. DOI: 10.1093/icesjms/fsp188.

Hart, D. R., Munroe, D. M., Caracappa, J. C., Haidvogel, D., Shank, B. V., Rudders, D. B., Klinck, J. M., Hofmann, E. E., and Powell, E. N. (June 2020). "Spillover of sea scallops from rotational closures in the Mid-Atlantic Bight (United States)". In: *ICES Journal of Marine Science* 77.5, pp. 1992–2002. ISSN: 1054-3139. DOI: 10.1093/icesjms/fsaa099.

Hart, D. R. and Rago, P. J. (2006). "Long-term dynamics of US Atlantic sea scallop *Placopecten magellanicus* populations". In: *North American Journal of Fisheries Management* 26.2, pp. 490–501. DOI: 10.1577/M04-116.1.

Hastie, T. J. and Tibshirani, R. J. (1990). *Generalized additive models*. Vol. 43. CRC press.

Hengl, T., Heuvelink, G. B., and Rossiter, D. G. (2007). "About regression-kriging: From equations to case studies". In: *Computers & Geosciences* 33.10, pp. 1301–1315. DOI: 10.1016/j.cageo.2007.05.001.

Hilborn, R. and Walters, C. J. (1987). "A general model for simulation of stock and fleet dynamics in spatially heterogeneous fisheries". In: *Canadian Journal of Fisheries and Aquatic Sciences* 44.7, pp. 1366–1369. DOI: 10.1139/f87-163.

Horrocks, J. and Rueffer, M. (2014). "A Bayesian approach to estimating animal density from binary acoustic transects". In: *Computational Statistics & Data Analysis* 80, pp. 17–25. DOI: 10.1016/j.csda.2014.06.005.

Howland, J., Gallager, S., Singh, H., Girard, A., Abrams, L., Griner, C., Taylor, R., and Vine, N. (2006). "Development of a towed survey system for deployment by the fishing industry". In: *OCEANS 2006*. IEEE, pp. 1–5. DOI: 10.1109/OCEANS.2006.307098.

Izquierdo, F., Paradinas, I., Cerviño, S., Conesa, D., Alonso-Fernández, A., Velasco, F., Preciado, I., Punzón, A., Saborido-Rey, F., and Pennino, M. G. (2021). "Spatio-Temporal Assessment of the European Hake (Merluccius merluccius) Recruits in the Northern Iberian Peninsula". In: *Frontiers in Marine Science* 8. ISSN: 2296-7745. DOI: 10.3389/fmars.2021.614675.

Jiao, Y., O'Reilly, R., Smith, E., Orth, D., and Ernesto Jardim, H. editor: (2016). "Integrating spatial synchrony/asynchrony of population distribution into stock assessment models: a spatial hierarchical Bayesian statistical catch-at-age approach". In: *ICES Journal of Marine Science* 73.7, pp. 1725–1738. DOI: 10.1093/icesjms/fsw036.

Kaplan, K. A., Hart, D. R., Hopkins, K., Gallager, S., York, A., Taylor, R., and Sullivan, P. J. (2017). "Evaluating the interaction of the invasive tunicate *Didemnum vexillum* with the Atlantic sea scallop *Placopecten magellanicus* on open and closed fishing grounds of Georges Bank". In: *ICES Journal of Marine Science* 74.9, pp. 2470–2479. DOI: 10.1093/icesjms/fsx076.

— (2018). "Invasive tunicate restructures invertebrate community on fishing grounds and a large protected area on Georges Bank". In: *Biological Invasions* 20.1, pp. 87–103. DOI: 10.1007/s10530-017-1517-y.

Lemoine, N. P. (2019). "Moving beyond noninformative priors: why and how to choose weakly informative priors in Bayesian analyses". In: *Oikos* 128.7, pp. 912–928. DOI: 10.1111/oik.05985.

Lenk, P. and Orme, B. (2009). "The value of informative priors in Bayesian inference with sparse data". In: *Journal of Marketing Research* 46.6, pp. 832–845. DOI: 10.1509/jmkr.46.6.832_JMR6J.

Levin, S. A. (1992). "The Problem of Pattern and Scale in Ecology: The Robert H. MacArthur Award Lecture". In: *Ecology* 73.6, pp. 1943–1967. DOI: https://doi.org/10.2307/1941447.

Meng, Q., Liu, Z., and Borders, B. E. (2013). "Assessment of regression kriging for spatial interpolation–comparisons of seven GIS interpolation methods". In: *Cartography and Geographic Information Science* 40.1, pp. 28–39. DOI: 10.1080/15230406.2013.762138.

Miller, T. J. (2013). "A comparison of hierarchical models for relative catch efficiency based on paired-gear data for US Northwest Atlantic fish stocks". In: *Canadian Journal of Fisheries and Aquatic Sciences* 70.9, pp. 1306–1316. DOI: 10.1139/cjfas-2013-0136.

Miller, T. J., Hart, D. R., Hopkins, K., Vine, N. H., Taylor, R., York, A. D., and Gallager, S. M. (2019). "Estimation of the capture efficiency and abundance of Atlantic sea scallops (*Placopecten magellanicus*) from paired photographic–dredge tows using hierarchical models". In: *Canadian Journal of Fisheries and Aquatic Sciences* 76.6, pp. 847–855. DOI: 10.1139/cjfas-2018-0024.

Naidu, K. and Robert, G. (2006). "Chapter 15 Fisheries sea scallop, Placopecten magellanicus". In: *Scallops: Biology, Ecology and Aquaculture*. Ed. by S. E. Shumway and G. J. Parsons. Vol. 35. Developments in Aquaculture and Fisheries Science. Elsevier, pp. 869–905. DOI: 10.1016/S0167-9309(06)80042-6.

NEFSC (2014). "59th Northeast Regional Stock Assessment Workshop (59th SAW) Assessment Report". In: *Northeast Fish Sci Cent Ref Doc* 14-09. URL: https://repository.library.noaa.gov/view/noaa/4803.

— (2018). "65th Northeast Regional Stock Assessment Workshop (65th SAW) Assessment Report". In: *Northeast Fish Sci Cent Ref Doc* 18-11. DOI: 10.25923/zapm-ga75. URL: http://www.nefsc.noaa.gov/publications/.

NOAA Fisheries (2022). *Commercial Landings*. Accessed: 2022-10-28. URL: https://www.fisheries.noaa.gov/foss/f?p=215:200:22227079719152:Mail::::.

Outeiro, L., Otero, J., Alonso-Fernández, A., Bañón, R., and Palacios-Abrantes, J. (2021). "Quantifying abundance trends and environmental effects on a population of queen scallop Aequipecten opercularis targeted by artisanal fishers in a coastal upwelling area (Ría de Arousa, NW Spain) using a Bayesian spatial model". In: *Fisheries Research* 240, p. 105963. ISSN: 0165-7836. DOI: https://doi.org/10.1016/j.fishres.2021.105963.

Puebla, O., Bermingham, E., and McMillan, W. O. (2012). "On the spatial scale of dispersal in coral reef fishes". In: *Molecular Ecology* 21.23, pp. 5675–5688. DOI: 10.1111/j.1365-294X.2012.05734.x.

R Core Team (2022). *R: A Language and Environment for Statistical Computing*. v. 4.1.3. R Foundation for Statistical Computing. Vienna, Austria. URL: https://www.R-project.org/.

Raftery, A. E., Lewis, S., Bernardo, J., Berger, J., Dawid, A., and Smith, A. (1992). "Bayesian Statistics". In: *Oxford Sci. Publ*, pp. 323–349.

Rodriguez, J. D., Perez, A., and Lozano, J. A. (2009). "Sensitivity analysis of k-fold cross validation in prediction error estimation". In: *IEEE Transactions on Pattern Analysis and Machine Intelligence* 32.3, pp. 569–575. DOI: 10.1109/TPAMI.2009.187.

Sale, P. F. and Ludsin, S. A. (2003). "The extent and spatial scale of connectivity among reef fish populations: implications for marine protected areas designated for fisheries enhancement". In: *Gulf and Caribbean Research* 14.2, pp. 119–128. DOI: 10.18785/gcr.1402.09.

Shackell, N. L., Fisher, J. A., Frank, K. T., and Lawton, P. (2012). "Spatial scale of similarity as an indicator of metacommunity stability in exploited marine systems". In: *Ecological Applications* 22.1, pp. 336–348. DOI: 10.1890/10-2093.1.

Shank, B. V., Hart, D. R., and Friedland, K. D. (2012). "Post-settlement predation by sea stars and crabs on the sea scallop in the Mid-Atlantic Bight". In: *Marine Ecology Progress Series* 468, pp. 161–177. DOI: 10.3354/meps09974.

Shepherd, T. D. and Litvak, M. K. (2004). "Density-dependent habitat selection and the ideal free distribution in marine fish spatial dynamics: considerations and cautions". In: *Fish and Fisheries* 5.2, pp. 141–152. DOI: 10.1111/j.1467-2979.2004.00143.x.

Stokesbury, K. D. and Himmelman, J. H. (1993). "Spatial distribution of the giant scallop *Placopecten magellanicus* in unharvested beds in the Baie des Chaleurs, Quebec". In: *Marine Ecology-Progress Series* 96, pp. 159–159.

Thorson, J. T., Shelton, A. O., Ward, E. J., and Skaug, H. J. (2015). "Geostatistical delta-generalized linear mixed models improve precision for estimated abundance indices for West Coast groundfishes". In: *ICES Journal of Marine Science* 72.5, pp. 1297–1310. DOI: 10.1093/icesjms/fsu243.

Thouzeau, G., Robert, G., and Smith, S. J. (1991). "Spatial variability in distribution and growth of juvenile and adult sea scallops *Placopecten magellanicus* (Gmelin) on eastern Georges Bank (Northwest Atlantic)". In: *Marine Ecology Progress Series*, pp. 205–218. URL: https://www.jstor.org/stable/24825825.

Tilman, D. and Kareiva, P. (1997). "Spatial ecology: the role of space in population dynamics and interspecific interactions". In: *Monographs in Population Biology*. Vol. 30. Princeton University Press. ISBN: 0-691-01653-4.

Truesdell, S. B., Hart, D. R., and Chen, Y. (2016). "Effects of spatial heterogeneity in growth and fishing effort on yield-per-recruit models: an application to the US Atlantic sea scallop fishery". In: *ICES Journal of Marine Science* 73.4, pp. 1062–1073. DOI: 10.1093/icesjms/fsv238.

Wagenmakers, E.-J., Morey, R. D., and Lee, M. D. (2016). "Bayesian benefits for the pragmatic researcher". In: *Current Directions in Psychological Science* 25.3, pp. 169–176. DOI: 10.1177/0963721416643289.

Wilen, J. E. (2004). "Spatial Management of Fisheries". In: *Marine Resource Economics* 19.1, pp. 7–19. DOI: 10.1086/mre.19.1.42629416.

Wood, S. (Jan. 2001). "mgcv: GAMs and generalized ridge regression for R". In: *R News* 1.

Wood, S. N. (2003). "Thin-plate regression splines". In: *Journal of the Royal Statistical Society (B)* 65.1, pp. 95–114. DOI: 10.1111/1467-9868.00374.

Xu, L., Chen, X., Guan, W., Tian, S., and Chen, Y. (2018). "The impact of spatial autocorrelation on CPUE standardization between two different fisheries". In: *Journal of Oceanology and Limnology* 36.3, pp. 973–980. DOI: 10.1007/s00343-018-6294-7.

Tables

Table 1: Results of a stratified mean (SM) design-based estimate (left), the frequentist GAM+OK (middle), and the Bayesian model (right). Regions are Mid-Atlantic Bight (MAB) and Georges Bank (GB). Abbreviations are given as in Figure 1. Abundance is given in millions. Range is given in meters.

		SM		**GAM+OK**					**Bayes+OK**				
Area	Region	Abundance	CV	Abundance	CV	Range	Sill	Nugget	Abundance	CV	Range	Sill	Nugget
DMV	MAB			2445	0.12	7318	0.20	0.07	2795	0.28	2430	2251	0.81
ET				8577	0.09	4947	5.10	0.00	9312	0.02	1692	19212	0.81
HC				2808	0.15	6718	0.36	0.00	2145	0.09	1510	5458	0.80
HCsr				2767	0.08	12384	0.08	0.02	2279	0.12	1736	517	0.77
LI				1949	0.13	704	0.11	0.04	1756	0.03	2156	218	0.78
Total		26797	0.03	18547					18288				
CA2_N	GB			198	0.38	11989	0.11	0.09	215	0.18	50266	364	0.79
CA2_S				1855	0.08	42676	0.19	0.00	1409	0.05	2164	765	0.77
GSC_E				416	2.59	788	14.75	3.36	344	0.45	1015	1262	0.79
GSC_S				16118	0.47	46733	152.10	64.54	20542	0.09	2091	8347	0.81
GSC_W				1465	0.28	12684	0.38	0.10	985	0.06	1930	3466	0.80
NF				109	0.55	178410	0.12	0.03	114	0.92	1485	52	0.78
SF				523	0.18	3037	0.04	0.00	753	0.09	729	13	0.62
Total		23884	0.02	20475					24362				

Figure Captions

Figure 1. Map of the study location, both regions, and all twelve areas. Regions are Mid-Atlantic Bight (MAB) and Georges Bank (GB). Areas are: Delmarva (DMV), Elephant Trunk (ET), Hudson Canyon (HC), Hudson Canyon southern rim (HCsr), Long Island (LI), Closed Area 2 North (CA2_N), Closed Area 2 South (CA2_S), Great South Channel East (GSC_E), Great South Channel South (GSC_S), Great South Channel West (GSC_W), Northern Flank (NF), and Southern Flank (SF).

Figure 2. Probability of presence as a function of cardinal direction for each area of each region. Abbreviations are given as in Figure 1. The cardinal direction is listed below the x-axis of each individual plot. Shaded areas are 95% high posterior density intervals. The lower and upper extremes of the x-axis represent the minimum and maximum value of the given cardinal direction within that area.

Figure 3. The relationship of mean density (m^{-2}) to depth. Abbreviations are given as in Figure 1. Shaded areas are 95% high posterior density intervals. Points are all density observations within a given area. The lower and upper extremes of the x-axis represent the minimum and maximum value of depth within that area.

Figure 4. The relationship of mean density (m^{-2}) to two-dimensional spatial coordinates. Abbreviations are given as in Figure 1.

Figure 5. Estimated mean, kriged residuals, and total estimated density (mean + kriged residuals; m^{-2}) arising from the Bayes+OK model (left; this study) and the GAM+OK model (right; Chang et al. (2017)) in the Mid-Atlantic Bight as a function of both depth and two-dimensional spatial coordinates. The estimates on the left arise from the Bayesian model presented here, while the estimates on the right arise from the frequentist model presented in Chang et al. (2017). Both the mean and the totals are given as the natural log offset by one in

order to emphasize fine-scale differences. The kriged residuals are given as the absolute value of the natural log offset by one. Those values which are negative on the linear scale are marked in red, while positive values on the linear scale are marked in blue, with increasing saturation indicating greater negative or positive values, respectively.

Figure 6. Estimated mean, kriged residuals, and total estimated density (mean + kriged residuals; m^{-2}) arising from the Bayes+OK model (left; this study) and the GAM+OK model (right; Chang et al. 2017) in Georges Bank as a function of both depth and two-dimensional spatial coordinates. The estimates on the left arise from the Bayesian model presented here, while the estimates on the right arise from the frequentist model presented in Chang et al. 2017. Both the mean and the totals are given as the natural log offset by one in order to emphasize fine-scale differences. The kriged residuals are given as the absolute value of the natural log offset by one. Those values which are negative on the linear scale are marked in red, while positive values on the linear scale are marked in blue, with increasing saturation indicating greater negative or positive values, respectively.

Figure 7. The root mean square error (RMSE) of the 10-fold cross-validation procedure for each subarea. We present the adjusted natural log in order to place all values on roughly similar scales. Stars mark the superior model (lower RMSE) among each pair. Abbreviations are given as in Figure 1.

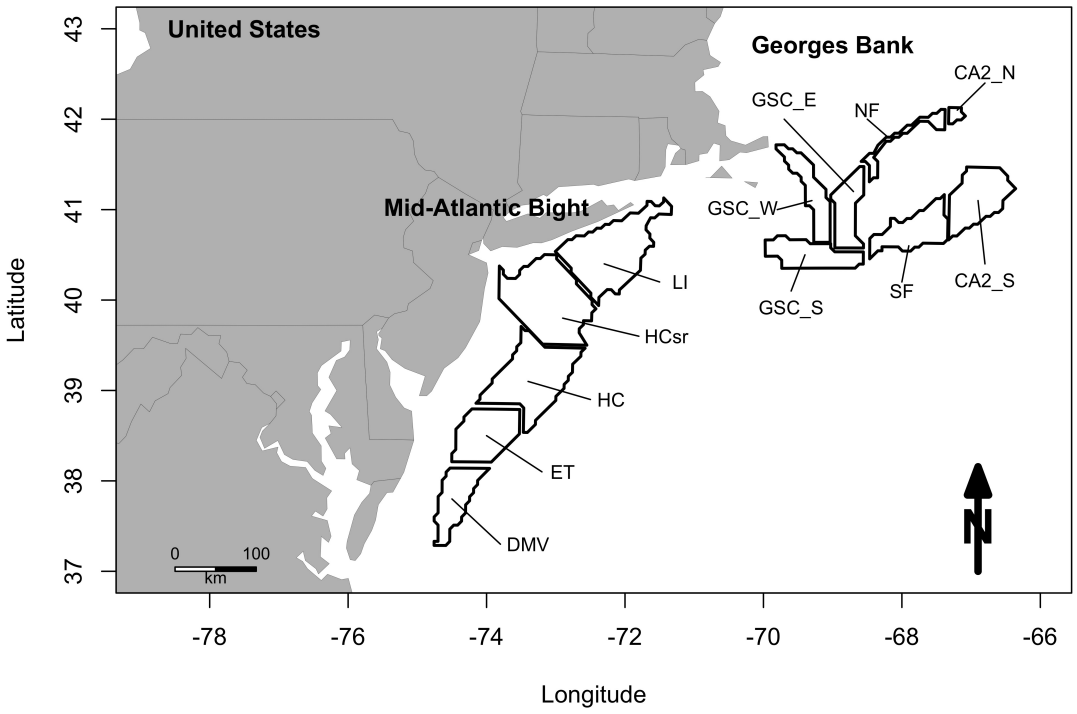
United States
Georges Bank
Mid-Atlantic Bight
CA2_N
GSC_E
NF
GSC_W
LI
HCsr
HC
ET
DMV
GSC_S
SF
CA2_S
0
100
km
N
Latitude
Longitude
43
42
41
40
39
38
37
-78
-76
-74
-72
-70
-68
-66

Figure 1

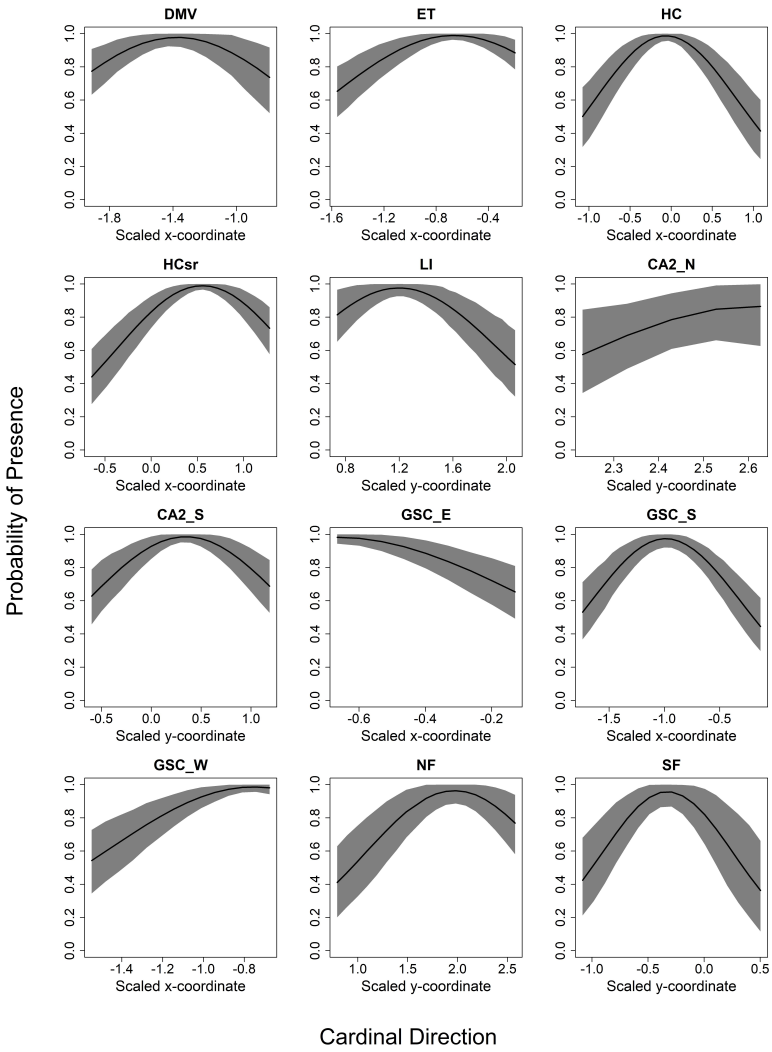
DMV
ET
HC
HCsr
LI
CA2_N
CA2_S
GSC_E
GSC_S
GSC_W
NF
SF
Probability of Presence
Scaled x-coordinate
Scaled y-coordinate
Cardinal Direction

Figure 2

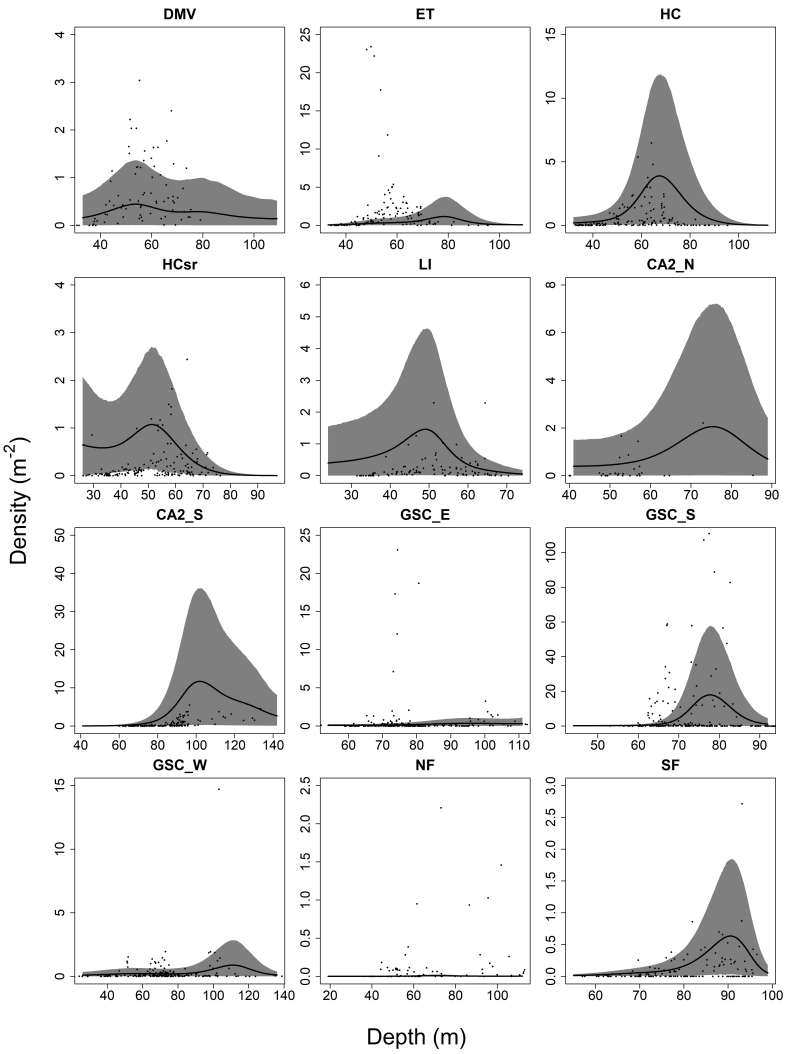
DMV
ET
HC
HCsr
LI
CA2_N
CA2_S
GSC_E
GSC_S
GSC_W
NF
SF
Density (m^{-2})
Depth (m)

Figure 3

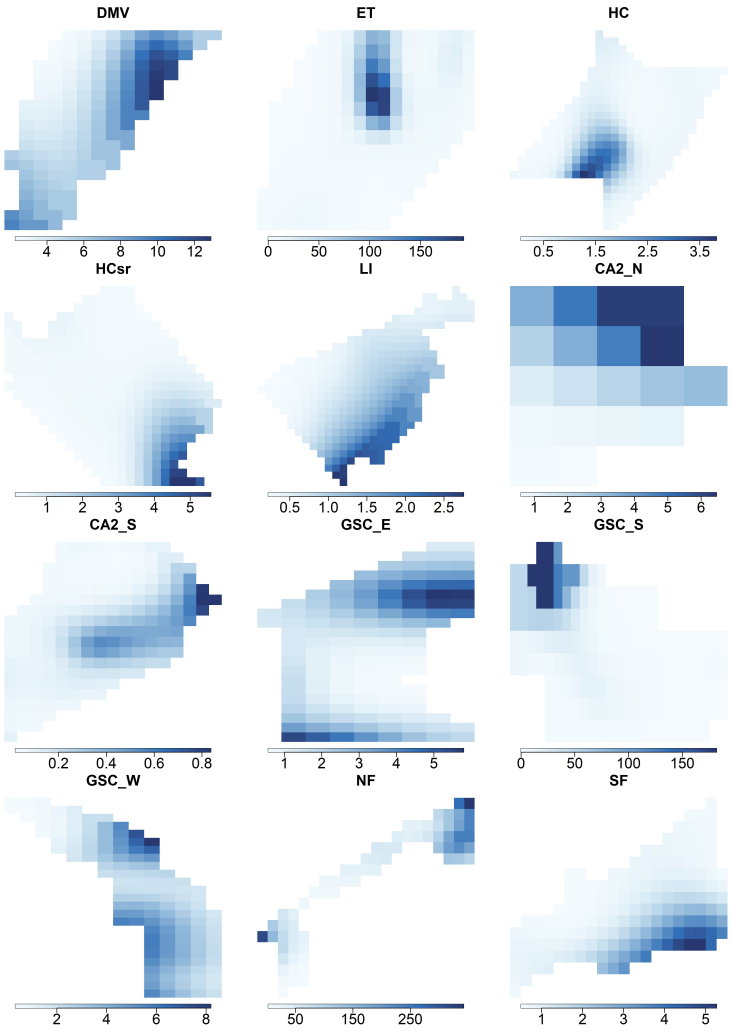
DMV
4 6 8 10 12
ET
0 50 100 150
HC
0.5 1.5 2.5 3.5
HCsr
1 2 3 4 5
LI
0.5 1.0 1.5 2.0 2.5
CA2_N
1 2 3 4 5 6
CA2_S
0.2 0.4 0.6 0.8
GSC_E
1 2 3 4 5
GSC_S
0 50 100 150
GSC_W
2 4 6 8
NF
50 150 250
SF
1 2 3 4 5

Figure 4

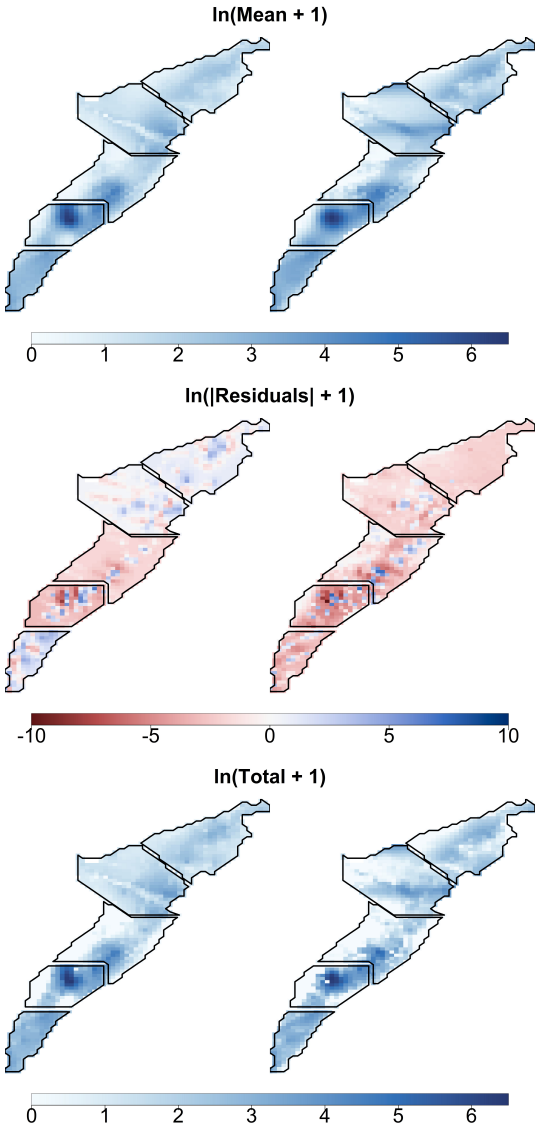

Figure 5

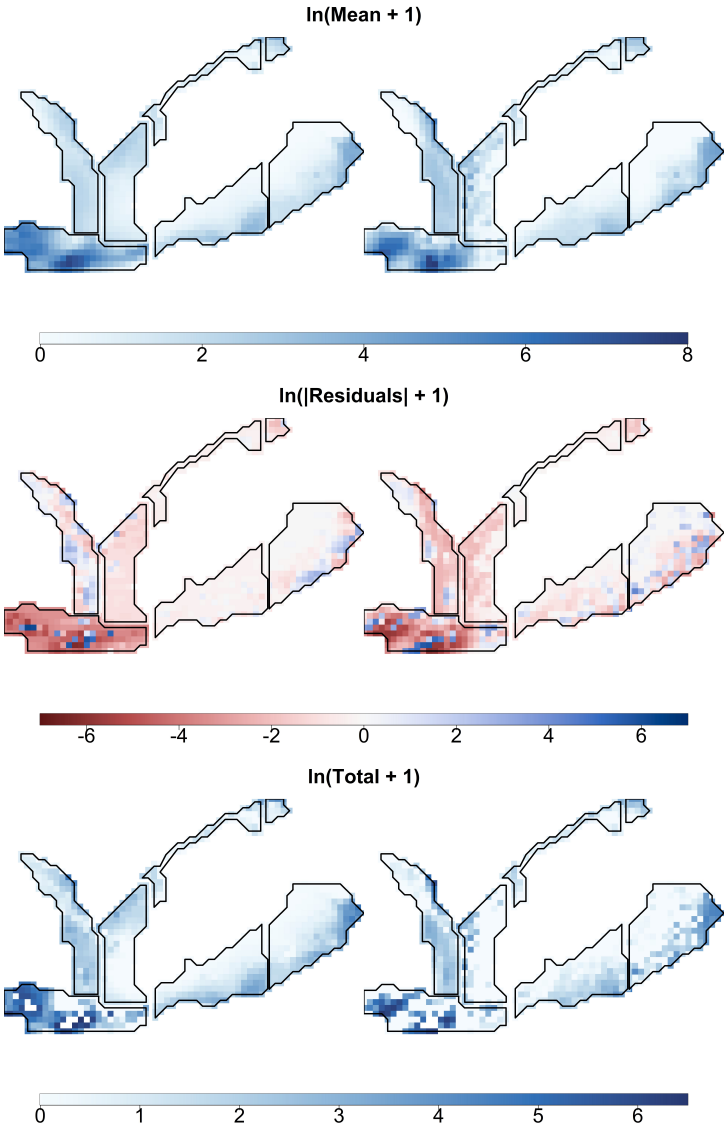

Figure 6

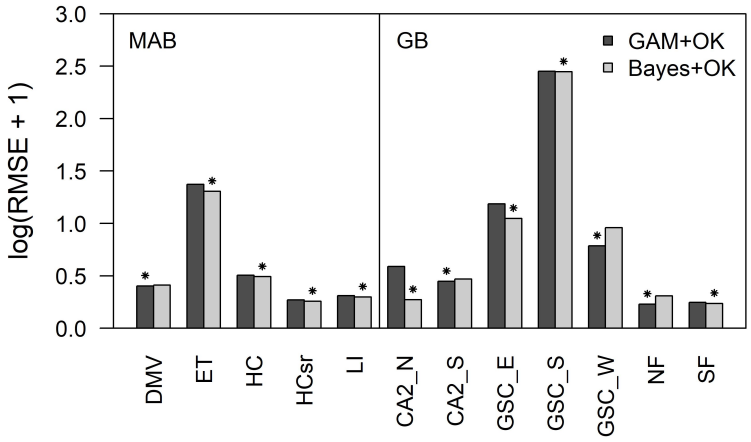
MAB
GB
GAM+OK
Bayes+OK
log(RMSE + 1)
3.0
2.5
2.0
1.5
1.0
0.5
0.0
DMV
ET
HC
HCsr
LI
CA2_N
CA2_S
GSC_E
GSC_S
GSC_W
NF
SF

Figure 7

Supplementary material

S1 Supplementary Figures

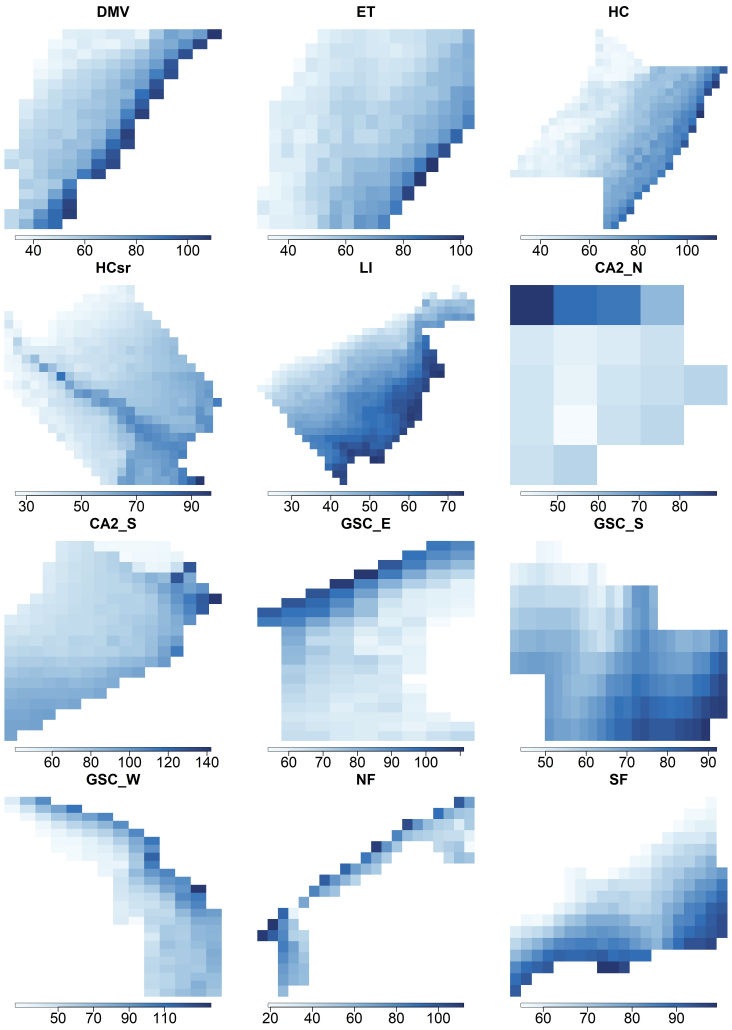

Figure S1: Observed depth (m) in each region. Abbreviations are given as in Figure 1 of the main text.

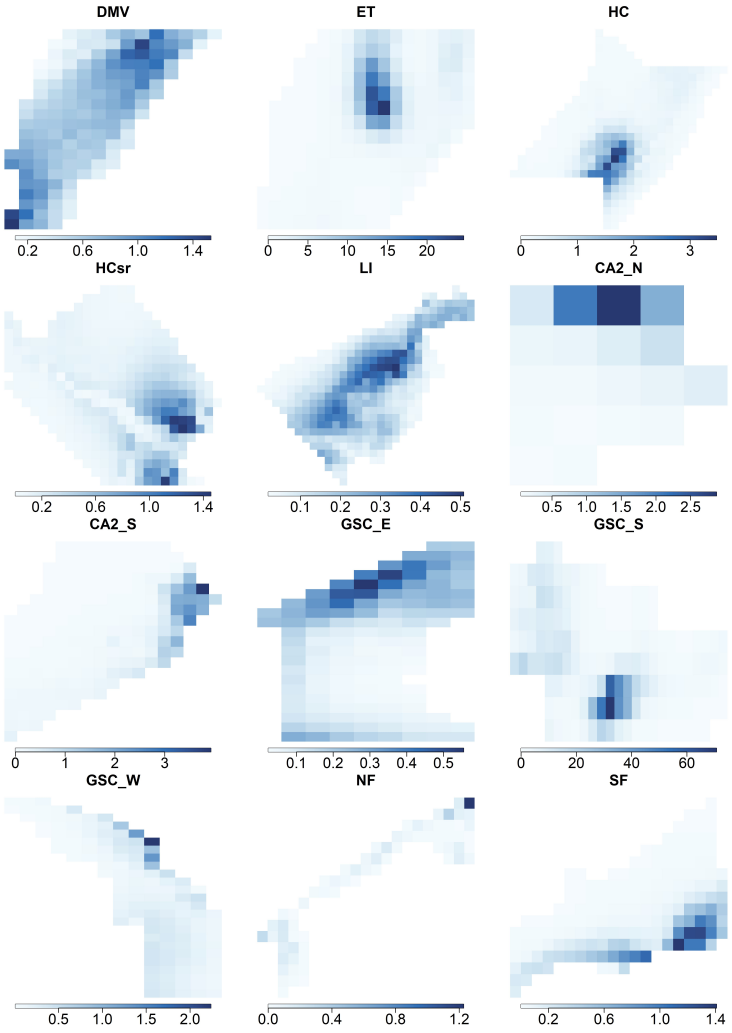

Figure S2: The relationship of mean density (m^{-2}) to both depth and two-dimensional spatial coordinates, and including probability of presence. Abbreviations are given as in Figure 1 of the main text.

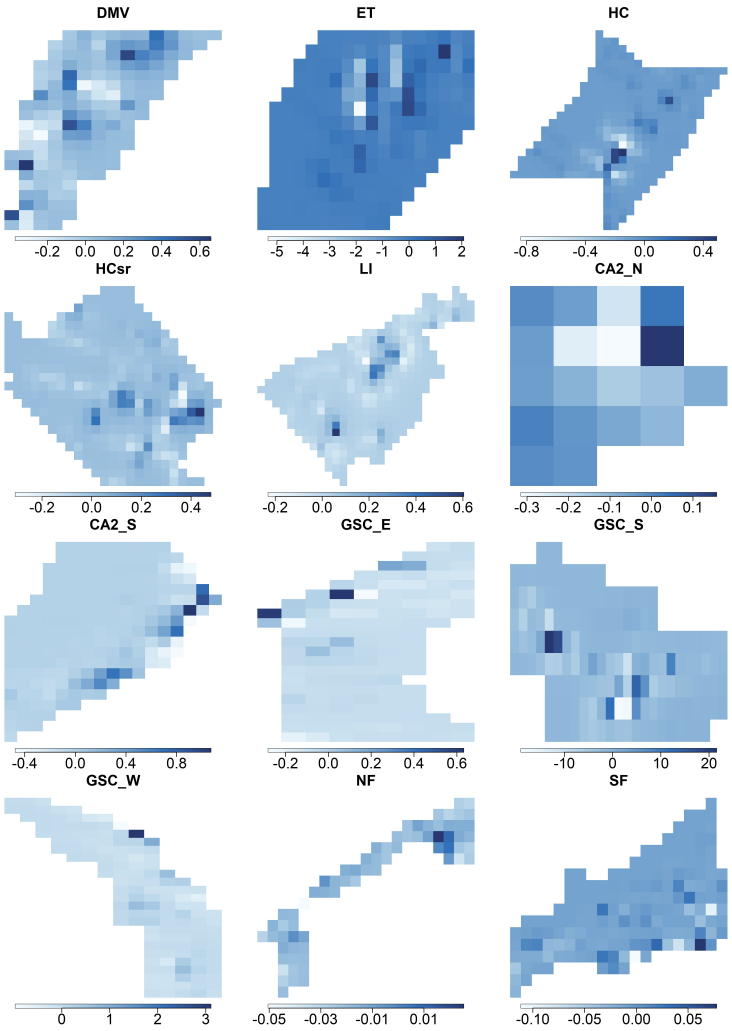

Figure S3: The kriged residuals (m^{-2}) for each region. Abbreviations are given as in Figure 1 of the main text.

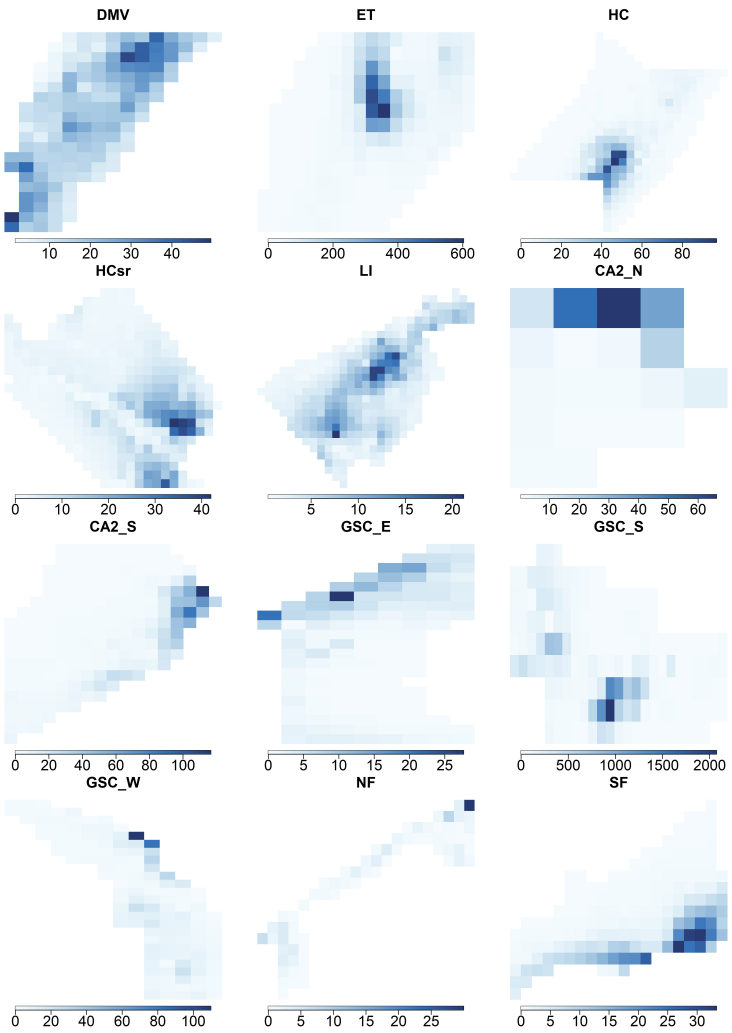

Figure S4: Final total density (m^{-2}) for each region. Abbreviations are given as in Figure 1 of the main text.

S2 Sensitivity Analysis

We performed a sensitivity analysis on the model results given prior choice by testing a small set of values for the variance of the prior distribution for each of the following parameters: nugget, sill, range, σ_d^2, and σ_c^2 (see equation 3 in the main text). This resulted in twenty additional model runs, which we performed as above, ultimately giving 6,000 samples for each model. All of these models converged ($\hat{R} < 1.1$), exhibited good mixing for each parameter, and had sufficient effective sampling sizes of more than 100 for the bulk and the tail, indicating adequate sampling of the mean, median, and upper and lower quantiles. Normal distributions truncated at zero were used for all of these parameters, with corresponding variances of 1 for all excepting the sill, which had a variance of 1000. For the sensitivity analysis, we tested prior variance values of 0.1, 1, 100, and 1000 for all five of these parameters, and monitored changes in the parameter posteriors, as well as the resultant median density and kriged residuals.

We determined whether posteriors across prior variance values were statistically different by assembling posterior probabilities of difference between posterior distribution pairs within a given test. That is, we sampled each pair of a given parameter's posterior distributions resulting from a given test – for example, all pairs of nugget posterior distributions across all four prior variance values for the range (Figure S5) – 6000 times and calculated the difference between each pair of values. If the confidence interval of the resulting distribution contained 0, we considered the pair of distributions to be statistically indistinguishable. We used the data set for Long Island (LI) for this sensitivity analysis, assuming similar results across all data sets.

The results of the sensitivity analysis suggest that the nugget is sensitive to its prior variance, but that it has no detectable effect on other parameters or the density and kriged residuals (see Figure S5). The range is very robust to changes in its prior variance, with high stability among other parameters as well. The sill is sensitive to very low values of the prior variance, while it appears to level out at higher values, suggesting that in practice low values would reflect a belief in a low magnitude of spatial autocorrelation. While there are apparent trends in the relative magnitude of the other parameters, none of the distributions are statistically distinguishable. The variance-inverse penalty of the spline coefficients, σ_d^2 and σ_c^2, are both sensitive to their prior variance, but this also results in statistically indistinguishable results for the other parameters.

The median density and kriged residuals of scallops are robust to changes in the parameters (Figure S5; bottom right). The only marked difference is in the highest posterior density interval of the median density in response to an increase in the posterior variance-inverse penalty of the depth cubic spline (σ_d^2). That is, increasing the prior variance of this parameter decreases our overall confidence in finding the median density within a given range of values. In practice, raising the prior variance of σ_d^2 may reflect a relative decrease in our confidence in the data.

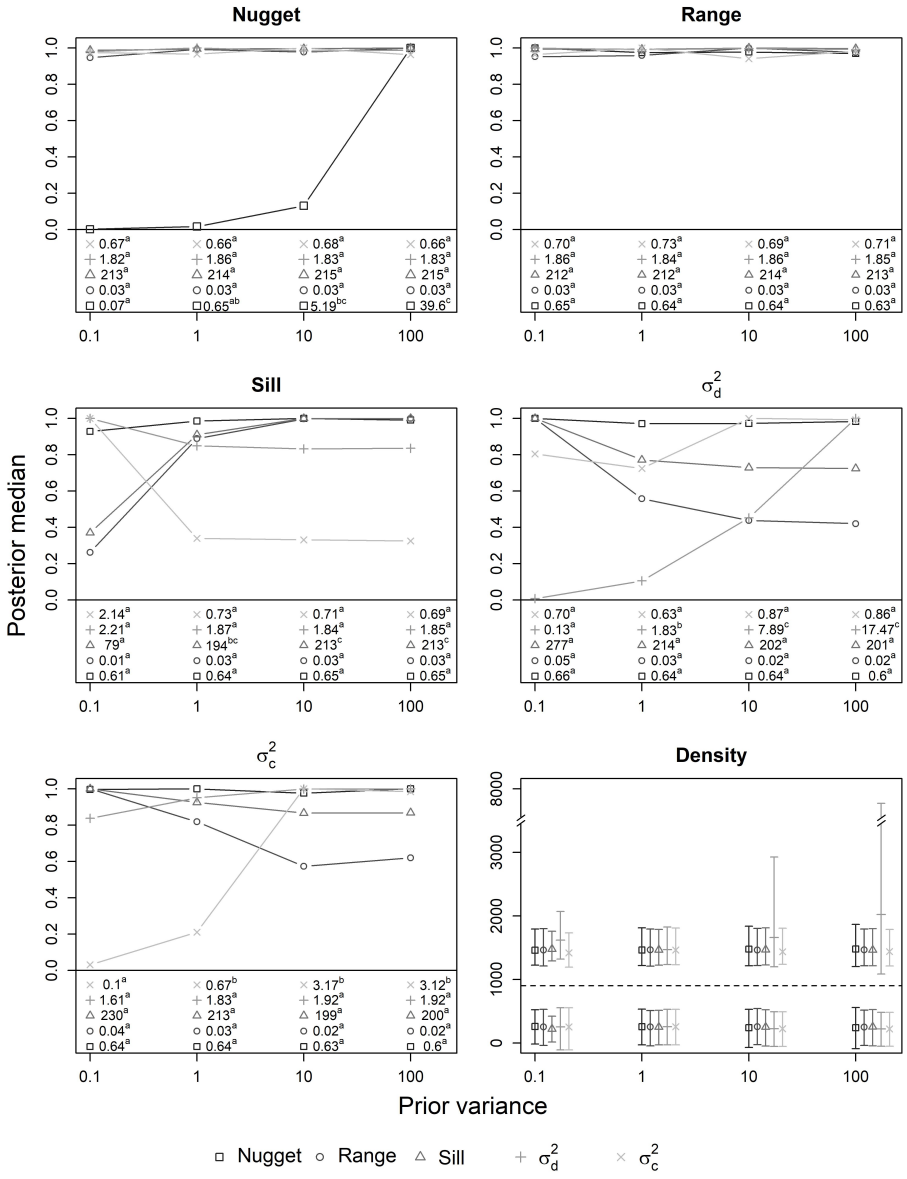

Figure S5: The response of model results to the prior variance of the nugget, range, sill, spatial thin plate spline variance-inverse penalty (σ_c^2), and depth cubic spline variance-inverse penalty (σ_d^2). The header of the five parameter plots reflect the altered prior distribution. We normalized the parameter results relative to the maximum of a given parameter. The values beneath these plots give the median of each parameter, marked by the relevant symbol. The four values accompanying a given symbol are marked with letters; those marked with the same letter are not statistically distinguishable. The density results (bottom right) give the mean and highest posterior density interval arising from the semi-parametric regression above and the kriged residuals below the dotted line. Note the broken y-axis of this plot. All density posteriors and all kriged residuals posteriors are statistically indistinguishable.

S3 Code and Data

Code to simulate data and run an analysis identical in character to the one presented in the main text can be found at https://github.com/epduskey/rkscallop. The code to replicate the analyses presented in this paper are available upon request from elizabeth.duskey@slu.se. The data are available upon request from Dvora Hart at deborah.hart@noaa.gov or Jui-Han Chang at jui-han.change@noaa.gov.